AgroScan: ISSN 0000-0000 (Online) 2023

Contents lists available at KulDevWeb

AgroScan

journal homepage: www.agroscan.kuldevpublication.com

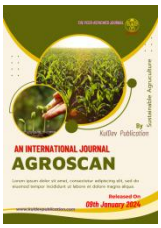

Research Article

Investigations on the Antibacterial Properties of *Cassia auriculata* Leaf Powder in the Synthesis of Silver Nanoparticles

*[1]Akash Nitin Gore and [2]Ramesh K. More

*[1]*Department of Agriculture, Kohinoor Arts, Commerce and Science College, Khultabad-431209, India*

[2]*Department of Agricultural Biotechnology, Government College of Science, Kishore, Maharashtra, India*

ARTICLE INFO

Article history:
Received 11 September 2023
Accepted 15 November 2023
Available online xxxx xxxx

Keywords:
Sonochemical
Antioxidant,
Heavy metal removal,
Ag nanoparticles,
Antibacterial

ABSTRACT

In current trends of nano drug research, the production of herbal nutritionally aided nanoparticles has a broad variety of applications of new non-side effect medical medications, as long as they are founded with environmentally acceptable methods. Sonochemical methods have been used to synthesis intermediated Silver (Ag) nanoparticles (NPs) from Cassia auriculata leaf, a traditional herbal used for phytochemical purposes. These approaches produce an ultra-sound effect. One of the greatest options in the current work on the green synthesis strategy is Ag nanoparticles, which may be used as a possible agent to study the antibacterial activity using the well diffusion method. Powder x-ray diffraction (PXRD) is a cornerstone quick analytic method in crystallography that determines the vital function of nanoparticle (NP) crystal size on both antimicrobial and heavy metal absorption, as well as other pertinent fundamental crystallographic data. The outcome showed that the prepared materials and Ag nanostructure were formed. (FTIR), Raman (FTR) and UV-Vis spectroscopy, respectively, are used to determine functional vibrations and optical results such as transmittance and absorption for a portion of the electromagnetic spectrum. Transmission electron microscopy (TEM) and selective area electron diffraction (SAED) methods are used to interpret information on the morphological characteristics and particle size of caped silver nanoparticles (NPs). The patterns obtained from these techniques are then used to show the nature of the size distribution and polydispersion..

Selection and peer-review under responsibility of scientific committee of editorial board members of AgroScan and author(s) and suggested reviewer.

Introduction

Recently, one of the most active and exciting research domains in solid-state physics, chemistry, and engineering has been nanomaterials. These materials are of basic importance because of their ability to radically alter a material's characteristics between the macroscopic (bulk materials) and modular (aggregates) scales. They also have potential uses as mechanical, optical, and catalytic technological artifacts. Conversely, a material's surface to volume ratio rise causes significant changes to its diffusion characteristics, such as segregation of grain boundaries and heterogeneous precipitation [1].

* Corresponding author.
E-mail address: akashgore66@gmail.com (Akash Nitin Gore)

https://doi.org/10
0000-0000/

Throughout history, silver has been prized for many of its beneficial qualities to humans. Among other things, it is used as a valuable commodity in coins, jewelry, decorations, electrical connections, and photography. Silver has been used for many years to great advantage as a strong antibacterial agent that is poisonous to viruses, fungus, and algae. Because of its broad-spectrum toxicity to germs and its reputation for having low human toxicity, silver has long been employed as a disinfectant, for example, in the treatment of burns and wounds [2].

Because of the increasing uses of these composites in optical, medical diagnostic, analytical chemistry, photocatalysis, and other fields, material scientists have focused a lot of emphasis on the development of novel nanomaterials including metal nanoparticles (Ag, Au, Cu, Rh, Pd, etc.) and their dopant. Numerous crystal forms of silver result in a range of fascinating physicochemical characteristics, including catalytic, electrochemical, optical, and electronic ones. The samples were heated to 100, 150, and 200°C in air for an hour in a furnace. The sample's XRD spectrum was captured using a PAN analytical X-ray diffractometer. The UV/Vis spectrum was recorded using a Schimadzu 160A twin beam spectrophotometer. When considering the natural and synthetic colors of common items, the optical behavior of materials, such as the selective absorption or reflection of certain visible spectrum portions, may be thought of as simply.

is a particular instance of how a solid reacts to the application of the electric and magnetic fields found in electromagnetic waves, such as light. At very high frequencies between 1014 and 1016 Hz, which correspond to wavelengths ranging from the infrared to the ultraviolet, this selectivity naturally extends beyond the range of wavelengths we can see into both the ultra violet and the infrared parts of the electromagnetic spectrum, where the difference arises due to the electric field strength [3]. At these frequencies, the selectivity changes alternatively in sign and amplitude.

The amplitude of the induced nuclear motion grows and the energy absorbed increases proportionately, reaching a maximum at the natural or resonant frequency when the frequency of the incoming wave is increased and approaches the lattice's inherent frequency of vibration. The nuclei's inertia causes the produced motion and energy absorption to diminish beyond that frequency. If the quantum of energy hυ is below the threshold for stimulating transitions of the electrons between permitted energy levels, then an optical wave of frequency much above the resonance frequency is transmitted with very minimal absorption of the lattice. Therefore, when examining the infrared spectra of insulators and semiconductors with band gaps in their electronic energy bands larger than photon energy, one may ignore the free electrons and just receive information on crystal lattice absorption. Nonetheless, even in the infrared spectrum, electrons predominate in metals and very narrow band gap semiconductors [4].

On the other hand, while nuclear mobility often may affect the effects that are noticed, the primary cause of the absorption and scattering of UV and visible radiations is the excitation of electrons into higher energy levels. Therefore, a useful tool for material scientists to utilize in the characterization of solids, liquids, and gases is the study of absorbed or emitted radiation as a function of wavelength. Thus, the electronic energy levels that may be analyzed include information on the local environment in which the atoms are located, in addition to being a property of the lattice and even the ionic species present. This could be explained if we acknowledge that (a) the number of occupied energy levels depends on the ionization state of an atom and (b) the solutions to Schrodinger's equation need to be slightly modified if the presence of neighboring ions modifies the potential distribution in and around the nucleus. [5].

RESOURCES AND TECHNIQUES

The leaf of Cassia auriculata (Fig. 1) was harvested, cleaned, sliced into tiny pieces, and dried for two weeks at room temperature (28±1°C). The leaf was then ground into a fine powder for further examination. Cassia auriculata leaf powder that had been shade-dried was extracted using 70% ethanol under reflux for eight hours, and the resulting semisolid mass was concentrated under decreased pressure using a Rotavapor apparatus made by Buchi Labortechnik AG in Switzerland. The result was a dark semisolid (greenish-black) substance with a yield of around 24% (w/w). Until it was utilized, it was kept at 4°C. The leftover extract was used for the

investigation when necessary and suspended in distilled water. Petroleum ether, chloroform, alcohol, acetone-water, and water were individually extracted from the air-dried, powdered plant material in a conical flask at room temperature. After boiling the whole ash that resulted from 2 grams of powdered leaves for 5 minutes with 25 milliliters of diluted hydrochloric acid, the insoluble material was gathered onto ashless filter paper [6]. It was lighted, weighed, and cleaned with hot water. A tarred glass container containing two grams of powdered Cassia auriculata leaf was used to weigh the sample initially. The sample was weighed after being cooked to 105°C in an oven. Using a JASCO UV-Vis-NIR (Model-V-670) spectrophotometer, ultraviolet–visible–near infrared (UV–Vis–NIR) spectra were recorded between 200 and 800 nm. Extreme pressure (100 atm) and temperatures (5000–50,000 K) are experienced during bubble collapse. Under these harsh circumstances, solute or solvent molecules within the bubbles break down and produce very reactive radicals.

Techniques for instrumentation

Using a Double beam UV-visible spectrophotometer (Specrtoscan UV-2600) with a 1 nm revolution between 300 and 700 nm, UV-visible spectral analysis was performed. The F-7000 FL spectrophotometer was used to detect fluorescence, and its scan speed was set at 1200 nm/min. A Bruker FTIR spectrophotometer was used to capture FTIR spectra in the 400–4000 cm–1 range. Bruker D8 advance XRD at 2θ degrees was used to investigate the dried powder of silver nanoparticles. Using a Quanta 200 FEG, scanning electron microscopy (SEM) was performed. Transmission electron microscopy (TEM - JEO2100) was used to investigate the size and crystalline nature of the nanoparticles. Using a CH silicone voltammetric analyzer model 604 E work station with three electrode systems, a cyclic voltammetric investigation was conducted [7].

Activity of antioxidants

Using the procedure outlined by (Blois 1958), the samples' capacity to completely eliminate the DPPH radical (1, 1-diphenyl-2-picrylhydrazyl) was assessed. A stock solution of 10 mg/ml of the chemical was made. An equivalent amount of varying extract concentrations (200, 400, 600, 800, and 1000 µg) was added to a 0.1 mM DPPH methanolic solution. After 30 minutes of room temperature incubation, the absorbance at 517 nm was measured for the reaction mixture. Three iterations of the experiment were conducted. Standard control was ascorbic acid. Using the following formula [8], the annihilation activity of free radicals was determined in percentage inhibition.

The bacterial pathogens Gram-Positive Staphylococcus Aureus (MTCC 96) was used for antibacterial activity. The origin of these particular pathogenic strains was the Microbial Type Culture Collection (MTCC), located in Punjab and Chandigarh, India.

Well diffusion techniques were used to assess the antibacterial activity [9]. As a positive control, the streptomycin addition worked well. The only negative control was the solvent itself. For twenty-four hours, the plates were incubated at 37 °C under a 40 W fluorescent light source (around 400 nm). Using an antibiotic zone scale (Himedia, Mumbai, India), the width of the zone of inhibition around the well was measured in order to assess the antibacterial activity. [10].

END RESULTS AND TALK

Characterization of structures

Regarding the structural analysis of nanopowder, PXRD is a crucial technique for determining the full width at the peak's half maximum, similarity to crystalline peak orientations, lattice and geometrical constants, purity among peak intensities, preferred orientation, as well as defects and stresses, among other things. The incident x-ray beam is presented with a sequence of parallel reflecting planes by the crystal lattice. At some angles, the path difference between two reflected waves from two separate crystal planes will maximize the intensity of the reflected beam when it is an integral multiple of λ. This requirement, known as Bragg's rule, is expressed as

follows: $n\lambda = 2d \sin\theta$, where θ is the x-ray wavelength, d is the distance between successive parallel planes, and θ is the glancing angle (or complement of the angle of incidence) [11].

Using the formula for the hexagonal crystal structure, the lattice parameter c of the as-deposited room temperature silver nanoparticle is determined and reported. The following formula relates the lattice parameter a to d for the cubic crystal system:

In this case, dhkl is the distance between two successive planes (m=1) with lattice plane index (hkl), an is a lattice constant, and h, k, and l are all integers. X-ray diffraction examination was performed utilizing an X'pert PRO (PANalytical) diffractometer with CuKα radiation and a scanning rate of 5° min-1 to ascertain the micro structural detail of the film.

Scherrer's equation, Crystallite size $D = k\lambda/ \beta \cos\theta$ (nm), was used to determine the average particle/grain size in Ag based on the X-ray diffraction data. The equation takes into account the grain size D, the full width at half maximum β, and the wavelength of the X-ray employed (1·5409$\bar{}$). Plotting the crystallite thickness and size at various annealing temperatures is shown in (Fig 2).

As demonstrated in Fig. 2, it is evident that the Ag NPs' diffraction pattern corresponds to a crystal system with distinctive diffraction peaks. According to JCPDS-ICDD Ref. C. No. 89-3722, the three distinct diffraction peaks at 2θ values of 38.043°, 44.530°, and 64.525° can be indexed to the (111), (200), and (220) reflection planes of the face-centered cubic structure of silver nanoparticles, respectively. It shows that the PXRD analysis verified the overall ensuing action of capping as well as size lowering agents of authorized herbal extract on the produced Ag NPs, as shown by the minor shift in the peaks from the standard data. It demonstrates that even if the PXRD findings and the SAED pattern correspond well, the PXRD scan area is much bigger because the former provides us with more relevant information while the latter performs diffraction on a group of particles [12].

SAED and TEM analysis

The composition, size distribution, structure, and morphology of the produced Ag NPs were quantitatively observed using a transmission electron microscope with excellent spatial resolution and analytical information.

As shown in (Fig 3a-b), the optical zoom of the TEM was measured as the ratio of the object's distance from the sample to the image's distance from the objective lens in the range of 20 nm and 10 nm magnification, respectively. The size distributions of Ag NPs revealed that the mean diameter of the nanoparticles ranged from about 30 to 10 nm, which confirms the face-centered cubic (FCC) crystalline structure of Ag NPs with negligible particle agglomeration and dispersion [13]. Every zone of the images shows that every particle scale ranging from higher nano dimension to lowers are crystalline as shown in the two observed images which reveal the polycrystalline NPs as well.

Figure 3(c) illustrates the explained SAED pattern that was seen on several zones of particle clusters. By comparing the related diffraction patterns from the JCPDS: ICDD (89-3722) worldwide diffraction database, phases were deduced [14].

DRS UV Spectroscopy or UV-Vis

Using a UV Visible spectrometer (Model: Shimadzu -1700 series) at room temperature, the UV–Visible optical absorption spectra of the green produced Ag NPs is shown in (Fig 4a). The transmission spectrum of the Ag nanoparticles only displays the reverse of the optical absorption spectra's curve, whereas the absorption spectra provides information about the sample's absorption of the incident light, with significant absorption seen at around 410 nm being regarded as greater absorption. Using the Tauc relation $\alpha = A(h\nu - Eg)1/2$, the optical band gap was computed and displayed between bandgap energy in eV and $(\alpha h\nu)2$, where α, h, ν, A, and Eg are the absorption coefficient, Plank's constant, photon frequency, amount of absorption in an arbitrary unit, and band

gap in eV, respectively. Figure 4 (a) UV-Visible absorption spectra shows the band gap curve for Ag NPs, which is determined to be 3.39 eV, which is closer to the published value of 3.2101 eV [15]. It is represented as the fluctuation of (αhν)1/n vs. photon energy (hν) with n = 1/2. (b) Green synthetic silver nanoparticles' UV–visible transmittance spectra as a function of wavelength. (c) The (**q**h*C*)2 vs h*C* curves for the green produced silver nanoparticles' optical band gap measurement

FTIR examination

The primary functional groups in the leaf extract may be measured and identified using FTIR, and their potential capping role in the production and stability of Ag NPs can also be determined. The infrared spectrum of a green produced Ag nano powder sample is shown in (Fig 5). It had many peaks rather than a single nosedive because leaf components were present, suggesting the complex structure of the phytomaterial. The stretching vibrations of OH stretching, C-H stretching, C-C stretching, C-H bending, and C-Ag vibrations were attributed to the bands that appeared at 3419, 2501, 1654, 1084, and 510 cm−1, respectively. There were some variations in the peaks compared to the established standard values of synthetic Ag Nps, indicating that leaf extract functional group confirmation acts as a capping agent in the Ag NP production process [16].

Raman analysis using lasers

Ag NPs may be effectively characterized in terms of their quality and structure using Raman spectroscopy. It works very well for figuring out the flaws and ordered and disordered properties of nanoparticles. Because the Raman and infrared spectra complement one another, some peaks that are absent are present here. The existence of alkyl silver functional groups is confirmed by the detected peaks at 166.37 cm-1, 271.03 cm-1, and 311.5 cm-1 (Fig. 6) [17].

Ag NPs' antioxidant qualities against DPPH

The DPPH free-radical scavenging ability of Ag NPs and C. auriculata leaf aqueous extract in a variety of doses shown remarkable protection in the current investigation, comparable to that of BHT as a conventional antioxidant agent. When compared to other molecules, free-radicals may accelerate a chemical process because they lack a full electron shell. They develop when radiation and tobacco smoke enter the human body. Oxygen is the most significant free radical in humans. Radiation exposure causes an oxygen molecule (O_2) to steal an electron from other molecules, damaging other molecules and DNA. Numerous chronic illnesses, including as cancer, diabetes, heart difficulties, and muscle failure, may be brought on by some of these alterations [18]. Antioxidants have been shown to be effective treatments for destroying free radicals and repairing damaged cells because they function like a broom against them. More significantly, research from laboratories has shown that antioxidants may effectively prevent cancer [19].

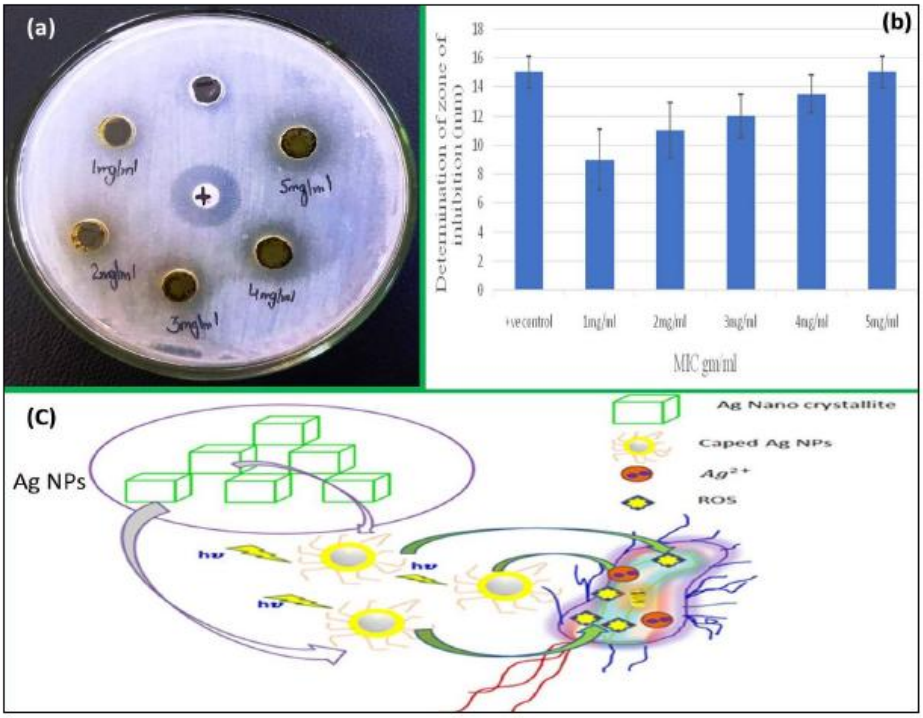

Fig 7(a) Photographic images which depict the inhibition zones formed around the well 7(b) Ejection of Ag^{2+} ions from the caped silver NPs (c) structure, size and shape of the prepared sample 7(c) Four chem-bio parameters involved in the proposed mechanism of antibacterial activity

The IC50 of the leaf aqueous extract of C. auriculata, BHT, and This fluctuation indicates that samples with different concentrations of antibacterial agents show increased efficacy against gram-positive bacteria. The following four chem-bio factors are included in the suggested mechanism of antibacterial action, as seen in (Fig. 7c): (Fig 7a) both the production of super ion entities and reactive oxygen species (Fig 7b) Ag2+ ions are expelled from the caped silver nanoparticles (c) according to the produced sample's size, shape, and structure. Excitons are created when electromagnetic waves with sufficient photon energy strike the bioculture environment around the sample, which in turn causes the production of ROS. Due to the activity of photo-exciton ROS, which may disturb the cell wall, nucleus, membrane, proteins, and DNA, the electromagnetic contact with the sample causes greater oxidative stress than the stress limit on the bacteria. This promotes cell destruction. Superradicals interact with cell walls and break them down to make it easier to enter or penetrate the cell domain. ROS has a noteworthy role in the antibacterial activity of the relevant sample. Larger S/V of particles is discovered to play a critical function in the zone of inhibition, leading to excellence of potential in antibacterial activities for certain great pharmaceutical candidates, according to TEM studies [23].

FINAL VERDICT

By adding Ag nanoparticles to the herbal leaf extract of C. auriculata, a sonochemical approach has proven effective in producing the desired results. The PXRD and TEM results combined with the SAED data showed a cubic structure free of any extra phases of contaminants, as well as the dimensions and shape of the particles. TheThe existence of phytochemical functional groups and their chemical connection with Ag are verified by the use of FTIR and Laser Raman spectra. After a thorough examination, this optimized silver nanoparticle shows strong antibacterial efficacy against gram positive staphylococcus aureus. Therefore, the produced green synthetic Ag NPs nanoparticles have found uses in pharmaceutical and biomedical flat form as well as in water purification procedures to prevent bacterial development.

References

1. Gao YZ, Chang TX, Wu YX. 2019. In-situ preparation and properties of bio-renewable acylated sodium alginate-g-polytetrahydrofuran/Ag-NPs nanocomposites. Applied Surface Science 483: 1027-1036.
2. Senthilkumar P, Yaswant G, Kavitha S, Chandramohan E, Kowsalya G, Vijay R, Sudhagar B, Kumar DRS. 2019. Preparation and characterization of hybrid chitosan-silver nanoparticles (Chi-Ag NPs); A potential antibacterial agent. International Journal of Biological Macromolecules 141: 290-298.
3. Oun AA, Rhim JW. 2017. Preparation of multifunctional chitin nanowhiskers/ZnO-Ag NPs and their effect on the properties of carboxymethyl cellulose-based nanocomposite film. Carbohydrate Polymers 169: 467-479.
4. Zayed MF, Eisa WH, Abdel-Moneam YK, El-Kousy SM, Atia A. 2015. Ziziphus spina-christi based bio-synthesis of Ag nanoparticles. Journal of Industrial and Engineering Chemistry 23: 50-56.
5. Duan C, Liu C, Meng X, Gao K, Lu W, Zhang Y, Dai L, Zhao W, Xiong C, Wang W, Liu Y. 2020. Facile synthesis of Ag NPs@ MIL-100 (Fe)/guar gum hybrid hydrogel as a versatile photocatalyst for wastewater remediation: Photocatalytic degradation, water/oil separation and bacterial inactivation. Carbohydrate Polymers 230: 115642.
6. Yazdi MET, Khara J, Housaindokht MR, Sadeghnia HR, Bahabadi SE, Amiri MS, Mosawee H, Taherzadeh D, Darroudi M. 2019. Role of ribes khorassanicum in the biosynthesis of AgNPs and their antibacterial properties. IET Nanobiotechnology 13(2): 189-192.
7. Rehan M, Mowafi S, Aly SA, Elshemy NS, Haggag K. 2017. Microwave-heating for in-situ Ag NPs preparation into viscose fibers. European Polymer Journal 86: 68-84.
8. Yang J, An X, Liu L, Seta FT, Zhang H, Nie S, Yao S, Cao H, Xu Q, Liu H, Ni Y. 2020. Chitin nano-crystals/sodium lignosulfonate/Ag NPs nanocomposites: a potent and green catalyst for efficient removal of organic contaminants. Cellulose 27(9): 5071-5087.
9. Luo S, Fan L, Yang K, Zhong Z, Wu X, Ren T. 2018. In situ and controllable synthesis of Ag NPs in tannic acid-based hyperbranched waterborne polyurethanes to prepare antibacterial polyurethanes/Ag NPs composites. RSC Advances 8(64): 36571-36578.
9. El-Nahrawy AM, Ali AI, Abou Hammad AB, Youssef AM. 2016. Influences of Ag-NPs doping chitosan/calcium silicate nanocomposites for optical and antibacterial activity. International Journal of Biological Macromolecules 93: 267-275.
10. Youssef AM, Hasanin MS, Abd El-Aziz ME, Turky GM. 2021. Conducting chitosan/hydroxylethyl cellulose/polyaniline bionanocomposites hydrogel based on graphene oxide doped with Ag-NPs. International Journal of Biological Macromolecules 167: 1435-1444.
11. Tippayawat P, Phromviyo N, Boueroy P, Chompoosor A. 2016. Green synthesis of silver nanoparticles in aloe vera plant extract prepared by a hydrothermal method and their synergistic antibacterial activity. Peer Journal 4: p.e2589.
12. Senthilkumar P, Yaswant G, Kavitha S, Chandramohan E, Kowsalya G, Vijay R, Sudhagar B, Kumar DRS. 2019. Preparation and characterization of hybrid chitosan-silver nanoparticles (Chi-Ag NPs); A potential antibacterial agent. International Journal of Biological Macromolecules 141: 290-298.
13. Divya M, Kiran GS, Hassan S, Selvin J. 2019. Biogenic synthesis and effect of silver nanoparticles (AgNPs) to combat catheter-related urinary tract infections. Biocatalysis and Agricultural Biotechnology 18: 101037.
14. Ren S, Zhao G, Wang Y, Wang B, Wang Q. 2015. Enhanced photocatalytic performance of sandwiched ZnO@ Ag@ Cu2O nanorod films: the distinct role of Ag NPs in the visible light and UV region. Nanotechnology 26(12): 125403.
15. Sikder M, Lead JR, Chandler GT, Baalousha M. 2018. A rapid approach for measuring silver nanoparticle concentration and dissolution in seawater by UV–Vis. Science of the Total Environment 618: 597-607.
16. Yang Y, Luo L, Li HP, Wang Q, Yang ZG, Long CL. 2016. Separation and determination of silver nanoparticle in environmental water and the UV-induced photochemical transformations study of AgNPs by cloud point extraction combined ICP-MS. Talanta 161: 342-349.
17. Jayaprakash N, Vijaya JJ, Kaviyarasu K, Kombaiah K, Kennedy LJ, Ramalingam RJ, Munusamy MA, Al-Lohedan HA. 2017. Green synthesis of Ag nanoparticles using Tamarind fruit extract for the antibacterial studies. Journal of Photochemistry and Photobiology B: Biology 169: 178-185.
18. Raza MA, Kanwal Z, Rauf A, Sabri AN, Riaz S, Naseem S. 2016. Size-and shape-dependent antibacterial studies of silver nanoparticles synthesized by wet chemical routes. Nanomaterials 6(4): 74.

19. Das G, Patra JK, Shin HS. 2020. Biosynthesis, and potential effect of fern mediated biocompatible silver nanoparticles by cytotoxicity, antidiabetic, antioxidant and antibacterial, studies. Materials Science and Engineering: C 114: 111011.
20. Chandhru M, Logesh R, Rani SK, Ahmed N, Vasimalai N. 2019. One-pot green route synthesis of silver nanoparticles from jack fruit seeds and their antibacterial activities with Escherichia coli and salmonella bacteria. Biocatalysis and Agricultural Biotechnology 20: 101241.
21. Majeed S, Danish M, Zahrudin AHB, Dash GK. 2018. Biosynthesis and characterization of silver nanoparticles from fungal species and its antibacterial and anticancer effect. Karbala International Journal of Modern Science 4(1): 86-92.
22. Gopinath PM, Narchonai G, Dhanasekaran D, Ranjani A, Thajuddin N. 2015. Mycosynthesis, characterization and antibacterial properties of AgNPs against multidrug resistant (MDR) bacterial pathogens of female infertility cases. Asian Journal of Pharmaceutical Sciences 10(2): 138-145.
23. Jaiswal S, Duffy B, Jaiswal AK, Stobie N, McHale P. 2010. Enhancement of the antibacterial properties of silver nanoparticles using β-cyclodextrin as a capping agent. International Journal of Antimicrobial Agents 36(3): 280-283.